DNA Traces on the Shroud of Turin: Metagenomics of the 1978 Official Sample Collection

Gianni Barcaccia [1] † *, Nicola Rambaldi Migliore [2] †, Giovanni Gabelli [1] †, Vincenzo Agostini [2], Fabio Palumbo [1], Elisabetta Moroni [2], Valeria Nicolini [2], Liangliang Gao [3], Grazia Mattutino [4], Andrew Porter [5], Pawel Palmowski [5], Noemi Procopio[6], Ugo A. Perego [7], Massimo Iorizzo [3], Timothy F. Sharbel [8], Pierluigi Baima Bollone [9], Antonio Torroni [2], Andrea Squartini [1], Alessandro Achilli [2] *

[1] Laboratory of Genomics, Research Centre for Agriculture "Maurizio Borin", Department DAFNAE, University of Padova; Campus of Agripolis, Legnaro (PD), Italy
[2] Department of Biology and Biotechnology "L. Spallanzani", University of Pavia; Pavia, Italy
[3] Plants for Human Health Institute, North Carolina State University, Kannapolis, NC 28081, USA
[4] Laboratory of Criminalistic Science "Carlo Torre", Department of Sciences of Public Health and Pediatrics, University of Torino; Turin, Italy
[5] Newcastle University Protein and Proteome Analysis (NUPPA) Facility, Medical School, Newcastle University, Newcastle upon Tyne, UK
[6] Research Center for Field Archaeology and Forensic Taphonomy, University of Lancashire, Preston, UK
[7] Southeastern Community College, West Burlington, Iowa 52655, USA
[8] Department of Plant Sciences, College of Agriculture and Bioresources, University of Saskatchewan, SK S7N 5A8, Canada
[9] Professor emeritus, University of Torino; Turin, Italy
†These authors contributed equally to this work

*Corresponding authors. Email: Gianni Barcaccia (ORCID ID: 0000-0001-7478-5048, Alessandro Achilli (ORCID ID: 0000-0001-6871-3451)
Email: gianni.barcaccia@unipd.it; alessandro.achilli@unipv.it

Author Contributions: Conceptualization: GB, AA; Data Curation: NRM, GG, AA; Formal Analysis: NRM, GG, VA, VN; Funding acquisition: AA, NRM, GB; Investigation: GB, NRM, GG, VA, FP, EM, AS, AA, MI, LG; Methodology: NRM, GG, VA, EM, AP, PP, NP; Project administration: GB, AA; Resources: GB, FP, GM, NP, PBB, AT, AA; Software: NRM, GG, VN; Visualization: GB, GG, VN; Supervision: GB, AT, AA; Validation: NRM, GG, AS; Writing – original draft: GB, AA; Writing – review & editing: GB, NRM, GG, FP, GM, UAP, TFS, PBB, AT, AS, AA, MI, LG.

Competing Interest Statement: The authors declare no competing interests.
Classification: Biological Sciences, Genetics; Social Sciences, Anthropology

Keywords: Turin Shroud, phylogenetics, ancient DNA, metagenomics, biodiversity.

This PDF file includes: Main Text and Figures 1 to 5

Abstract

This research provides original insights into the diversity of DNA extracted from samples collected in 1978 from the Turin Shroud, revealing its biological complexity through rigorous DNA and metagenomic analyses. Our findings highlight its preservation conditions and environmental interactions, offering valuable perspectives into the identified genetic variants, which originated from multiple biological sources. Several human mitochondrial DNA (mtDNA) lineages were identified, including K1a1b1a, which matches the 1978 official collector's mitogenome, H2a2 (*i.e*. the lineage of the mtDNA reference sequence rRCS), H1b, which is common in Western Eurasia, and H33, which is prevalent in the Near East and frequent among the Druze. Moreover, the reconstructed microbiome of the Shroud reveals a rich tapestry of multiple microbes commonly found on the human epidermis, as well as archaeal communities adapted to high salinity, and fungi including molds. This is indicative of the Shroud's preservation conditions over the centuries. Additionally, the presence of abundant Mediterranean endemic red coral, various cultivated plants (*e.g*. carrot, wheat, corn, bananas, and peanuts) and domesticated animals (*e.g*. cattle, pigs, chickens, dogs, and cats) provide a fascinating glimpse into the diverse biological sources of the contaminants that have accumulated on the Turin Shroud over time. Finally, radiocarbon dating of two distinct threads collected from the reliquary provides evidence of their use to repair the Shroud in the years 1534 and 1694 of the Common Era (CE).

Significance statement

An in-depth metagenomic analysis was conducted on several linen strands collected from different areas of the body image of the *Man of the Shroud* during the official sampling in 1978. Our analyses revealed several human mtDNA lineages, including one common in Western Eurasia and another prevalent in the Near East. Additionally, the diversity of animal and plant species identified details the significant environmental contamination of the Shroud that likely occurred in recent centuries, particularly following the voyages of Marco Polo and Christopher Columbus. Radiocarbon dating of two distinct textile residuals from the Shroud's reliquary indicated a time range between 1451 and 1800 CE, overlapping with the period of its repair interventions.

Main Text

Introduction

The Shroud of Turin is a linen burial cloth, approximately 4.4 meters long and 1.1 meters wide, which shows the double bodily image, front and back, of a man who has apparently suffered physical trauma through crucifixion with signs that are interpreted and believed to be compatible with those described in the New Testament (1, 2). It has been venerated for centuries, especially by members of the Catholic Church, and popular belief has this artifact as the cloth used to wrap the lifeless body of the biblical Jesus of Nazareth, who is acknowledged as the founder of the Christian movement that started in the Judean region in the mid-first century Common Era (CE).

The true nature of the Shroud has been highly debated among historians, theologians, and scientists. Several hypotheses regarding its origin have been proposed, but as of today, no one has yet been able to establish to any degree of certainty when and where this textile originated from. The only historical fact that has been recorded is that the Shroud has been in Europe since the mid-14th century, when it first appeared in Lirey, France, between 1353 and 1357. Starting in 1453, it was kept in Chambéry by the Dukes of Savoy until 1578, followed by several moves between France and the northern part of Italy during the 16th century, with the final resting place in Turin. Kept in a reliquary from 1694 to 1993, the Shroud was held permanently in the chapel adjacent to the Turin Cathedral, except for a brief move to Genoa in 1706 and to Montevergine, in the province of Avellino, during the Second World War. After a fire in the chapel in 1997, the Shroud was moved to the left chapel in the transept of the Turin Cathedral (for details, see (3–5)).

Considering available information and material, it has not yet been possible to either confirm or refute that the Shroud existed before its appearance in France in the mid-14th century. However, a commonly held belief is that its journey through the years began in Jerusalem, in a tomb in the Holy Land, approximately 2000 years ago, in the year 31 or 33 CE ((4) and references therein). Tradition narrates that after it was concealed for years, the Shroud would have been kept in what is modern-day Turkey, first in Mesopotamia then in Edessa, followed by a transfer to Şanliurfa, possibly around 200 CE. Subsequent moves would have seen the Shroud in Anatolia, Constantinople (modern-day Istanbul), in 944 CE (5). A burial cloth, which some historians believe to be the Shroud, was owned by the Byzantine emperors but disappeared during the sacking of Constantinople in 1204 CE (6). After this event, presumably the Shroud would have been taken by crusaders and transferred to Athens, Greece, where it would have remained until 1225. However, there are no official documents that support the presence of the Shroud in any of the above-mentioned locations.

Iconographic representations on Byzantine coins, the so-called gold *solidi* used during the Eastern Roman Empire, portray the face of the Man of the Shroud during the time of Justinian II, the Byzantine emperor who lived between 669 and 711 CE.

Numismatic experts believe that the engraver must have seen the Shroud before creating the image shown on this coin because of some distinctive facial traits in common with the sacred relic. Among the various historical proofs, it is worth mentioning the votive medallion of Lirey, found in France, which shows the frontal and dorsal image of the Man of the Shroud, probably dated between 1356 and 1370. In 1988, the age of the linen cloth of the Shroud of Turin was assessed by accelerator mass spectrometry, and results of radiocarbon measurements from separate independent laboratories yielded a calendar age range of 1260-1390 CE, thus suggesting a recent Medieval origin (7). However, the raw data of the radiocarbon measurements were not initially released and only in 2017 were they made accessible through the British Museum. Statistical analysis of the original raw data strongly suggests an absence of homogeneity between the datasets made by the three laboratories, which may have undermined their reliability (8), thus requiring additional testing to ascertain its age.

The possible existence of the Shroud prior to the first documented information places the long journey of this artifact into a Middle or Near East geographical context, with a potential historical age preceding the Sacking of Constantinople in 1204. This would have then been followed by a Western European relocation and subsequent reappearance at Lirey in 1353 or 1356. Our current study attempts to differentiate between the two referenced periods separated by the so called “missing years”, considering the two geographical areas characterized by distinctive genomic data associated with human lineages, plant species, or/and animal breeds. Furthermore, we divide the chronological history of this artifact into “pre-1204”, which could involve any geographical area of the ancient Near East, and a plausible “post-1353” location in western Europe. These two hypothetical temporal and spatial differentiations may be reflected in the variation of DNA data obtained from the Shroud.

Genomic DNA was previously isolated and analyzed from organic residues recovered in 1978 from different parts of the body image on the back of the Shroud, and from threads taken from the edges and used in 1988 for radiocarbon dating of this sacred artifact (9). Analysis of the DNA extracted from organic particles and textile strands sampled from the Shroud revealed chloroplast and mitochondrial genome sequences representing multiple plant species, as well as various human biogeographical origins. In particular, these analyses revealed the presence of at least 19 plant species common in the Mediterranean Basin, in addition to plants whose primary center of origin is Asia (China), the Middle East, and the Americas, some of which reflects their introduction to the Old World after the 12th century. In addition, the analyses revealed sequences from at least 14 people of different geographic ancestry, based on the Eurasian haplogroups identified which are common to Western Europe and North-eastern Africa, as well as from the Middle East, the Arabian Peninsula, the Caucasus region, and also rare haplotypes from the Indian sub-continent (9). A quantitative assessment of the overall amplicon sequencing data revealed that over 55.6% of the human DNA corresponds to lineages from the Near East, while Western European lineages account for less than 5.6%. The presence of 38.7% of the overall human genomic data from Indian

lineages is unexpected and is potentially linked to historical interactions associated with importing linen or yarn from regions near the Indus Valley, referred to as "Hindoyin" according to rabbinic texts (10).

The present study aimed to isolate and characterize genomic DNA sequences from Turin Shroud samples using a different molecular methodology (NGS vs. PCR) and an original sample consisting of linen filaments collected in 1978 by the late Prof. Pierluigi Baima Bollone from various sections of the Turin Shroud (11, 12). After DNA extraction in clean rooms, shotgun genomic libraries were sequenced using an NGS strategy with the main goal to determine the quantity and quality of human DNA and any residual DNA from microbial, fungal, plant, and animal species. The genetic results obtained were then correlated with historical information, the corresponding geographical areas of origin, and the modern distribution of plant species and human geographic groups with the aim of acquiring new data and providing novel clues as to the origin of the Shroud of Turin.

Results and Discussion

Human DNA sequences identified on the Turin Shroud

Before testing a total of twelve samples collected from the Turin Shroud (TS) (Table S1 and Figure S1), we verified the possibility of isolating and sequencing human DNA fragments from a linen cloth that had been purposely contaminated by touch. We obtained a low-coverage genome (2.5×) from the human control (lab operator; Dataset S1A).

We extracted DNA, built genomic libraries and obtained genomic reads from seven TS samples (Figure 1 and Dataset S1B). The percentage of trimmed reads that mapped to the human reference genome exceeded 10% in three cases, resulting in an average depth higher than 0.5× (higher than 1× for AB1 and B12). The average length of the reads (less than 100 base pairs) is consistent with the characteristics of degraded, possibly ancient DNA. However, both the damage patterns and the contamination tests show clear signatures of modern DNA contamination (Dataset S1B), as expected given the large number of people who have come into contact with the TS. To further characterize the possible presence of ancient DNA, we extracted, from each sample, reads showing patterns of deamination at their terminal bases. We applied the maximum-likelihood probabilistic model implemented in PMDtools (13) to assign post-mortem damage (PMD) scores to each read. The distribution of PMD scores is very similar among the seven samples, with most reads (>98.3%) showing a score lower than 1 (Figure S2). Only a small fraction showed PMDs greater than 3 (0.21% - 0.53%), which could be considered the minimum threshold for reliable ancient reads. For a threshold of PMDs > 5, between 0.05% and 0.19% of the total sequences were retained, comparable to values found in modern and historical individuals (13). An example of the damage patterns at different PMD scores is reported in the supplementary information for sample AB1 (Figure S3).

168 The genetic sex of these samples was determined to be likely that of a biological
169 male (Dataset S1B), and a predominant mitochondrial DNA (mtDNA) haplogroup
170 was determined with high accuracy (Q>0.95; Dataset S2A) in samples AB1, B12,
171 and C10-gl. This haplogroup, corresponding to K1a1b1a, is a typical Ashkenazi
172 subclade of K1a1b1 with a likely Western European origin (14). The same
173 haplogroup was identified by analyzing the mitochondrial genome of the late Prof.
174 Baima Bollone (the collector) (Dataset S2B). Therefore, we performed kinship
175 analyses, which revealed a close relationship (same individual or first-degree)
176 between the three TS DNAs and the genome of the collector, who has Jewish
177 ancestry (Table S2). As a negative control, we confirmed the complete
178 unrelatedness between the TS genomic data (and the collector) and the modern
179 linen specimen, artificially contaminated by the operator.
180 Other haplogroups were also identified in the three samples (Figure 1 and S4),
181 namely H2a2, H33 and H1b. The first two were also reported by Barcaccia *et al*.
182 (9). H2a2 is expected since it is the lineage of the mitochondrial reference
183 sequence rRCS (NC_012920) and therefore can be identified in any sample
184 without distinctive haplogroup markers. H1b is commonly found in Europe, and to
185 a lesser degree also in Central Asia (15). H33 is a rare haplogroup found today
186 mainly in the Near East, especially among the Druze, an Arabic-speaking ethno-
187 religious minority currently present in the Holy Land, Jordan, Lebanon, and Syria
188 (16, 17). Although several of the previously reported mitochondrial variants were
189 identified among the heteroplasmies (Dataset S2A), no additional haplogroups
190 could be identified with high accuracy. This is due to the high-quality filtering used
191 for variant calling (*i.e.*, 176 heteroplasmic variants are excluded from the final
192 haplotypes) and the ability to analyze entire mitogenomes, which greatly increases
193 the accuracy of classification, up to more than 70% (18). Our results indicate that
194 the human DNA found on the TS specimens mostly derives from the main
195 collector, and shows variable level of additional contamination.
196

197 ## Proteomics analyses

198 We used liquid chromatography–tandem mass spectrometry to analyze the
199 peptide profiles of three TS samples (namely, C/D12, B12, and R58). After
200 excluding four proteins identified in the negatives—keratin type II cytoskeletal 1,
201 triosephosphate isomerase, actin, and trypsin (deemed normal contaminants or
202 deliberately added to the sample)—and other common contaminants, such as
203 myosin and keratins 9 and 10, the only unique proteins identified in the C/D12 and
204 R58 samples were proteinase K, with 16 unique peptides identified overall, and
205 collagen alpha-1(I) chain, with two unique peptides identified in the R58 sample
206 (Dataset S3). The presence of proteinase K in the samples was expected because
207 the TS samples had been treated with proteinase K during previous attempts at
208 DNA extraction. Since the peptides of the collagen alpha-1(I) chain showed no
209 modification, they likely originated from skin contamination rather than from ancient
210 peptides. This is further supported by the high presence of keratins, which are
211 much higher in the samples than in the negative controls, indicating poor handling
212 procedures rather than issues associated with laboratory analysis. Overall, it can

213 be concluded that no ancient peptides were identified in the samples, only keratins
214 and other proteins associated with skin handling.
215
216 ## Radiocarbon Dating
217 Two linen threads collected from the reliquary were quantitatively sufficient for 14C
218 radiocarbon dating (R58-1 and R58-2, respectively), which was outsourced to the
219 Curt-Engelhorn-Zentrum Archäometrie (CEZA) in Mannheim, Germany (Figure
220 S5). The obtained ages (Dataset S1C) are consistent with two historical events.
221 The time range of sample R58-1 (1451-1622 CE) overlaps with the fire that broke
222 out in 1532 CE in the Chapel of Saint-Chapelle in Chambéry, where the Turin
223 Shroud was being kept inside a silver reliquary. The intense heat caused by
224 contact with molten silver burned through the folded cloth. The Shroud was saved
225 from destruction, and in 1534 CE, Poor Clare nuns repaired the burn holes by
226 sewing linen patches over the damaged areas (19). Further conservation mending
227 work was carried out in 1694 CE, likely under the direction of Sebastian Valfrè, to
228 stabilize the Shroud (20). This work overlaps with the time range of sample R58-2
229 (1642-1800 CE).
230
231 ## Metagenomics analyses
232 Due to the low number of reads from the Turin Shroud samples that mapped to the
233 human reference genome, we conducted a comprehensive metagenomic analysis.
234 We utilized the Kraken program for the initial screening. The distribution of reads
235 across kingdoms varied significantly (Table S3, Dataset S5), with unassigned
236 reads ranging from 17% (AB1) to 72% (R58). Reads assigned to viruses and
237 archaea were minimal, while bacterial species consistently accounted for 10% to
238 31% of the reads. The percentages of eukaryotic reads differed significantly and
239 showed an inverse relationship with unassigned reads; samples with fewer
240 unassigned reads had a higher proportion of eukaryotic reads and *vice versa*.
241 Regarding the eukaryotic reads, the vast majority were assigned to the genus
242 *Homo*: 93% or more in AB1, C/D12, C10_gl, and B12; 86% in C3_ha; and 77% in
243 R58 (Dataset S4). A notable exception was sample C12_fe, containing only 0.4%
244 eukaryotic reads, of which 26% were assigned to *Homo*. As in the other samples,
245 most of the remaining reads were assigned to Viridiplantae (e.g., 61% in the case
246 of C12_fe).
247 The data derived from the Kraken classification enabled identification of Bacteria,
248 Archaea, and Fungi, but were insufficient for Metazoa and Viridiplantae analyses
249 due to limited sequence databases. Therefore, we adopted an alternative
250 approach based on aligning the sequences against the NCBI nt database.
251 Because running BLAST on all individual reads was not feasible due to their high
252 number and short length, we performed a metagenomic assembly of the reads and
253 subsequently aligned the resulting contigs to the database using BLAST.
254 Challenges due to species diversity and DNA degradation resulted in low assembly
255 metrics and short contigs (with an average length of 210-250 nt, Table S4). The
256 results of the BLASTn analysis were categorized as those from Kraken (Table S5),

showing comparable trends with generally fewer unassigned contigs due to the larger NCBI nt database used. Samples R58 and C12_fe were exceptions with higher unassigned contig shares (83.8% and 95.1%, respectively). Both archaea and viruses were present only in trace amounts. Compared to the Kraken analysis, eukaryotic contig proportions increased in all samples, likely because of assembly biases that favored the abundant *Homo sapiens* genome. A significant number of bacterial contigs could not be classified at the species or phylum levels. Only a few archaea taxa were detected (a maximum of 28 in B12 and none in R58).

The fungi kingdom was used for comparison in the analyses. Identified orders showed strong similarity across samples, although less represented orders exhibited some variability. Kraken was deemed more reliable for species quantification, while BLAST performed better for species identification despite potential false negatives.

The Kraken results were further validated through an additional analysis with MetaPhlAn, a tool specifically designed to profile microbial communities from metagenomic shotgun sequencing (21). Unlike Kraken, which uses k-mer analysis across entire genomes, MetaPhlAn aligns unpaired reads to a comprehensive microbial gene database for precise identification. Consequently, MetaPhlAn identified fewer reads, with unclassified readings from 44% (AB1) to 99% (R58 and C12_fe). The detected taxa mostly aligned with the findings derived from Kraken analysis, identifying minimal archaea and the same bacterial classes. New species constituted only 2–4% of the reads in samples R58 and C12_fe, and were attributed to *Geobacillus jurassicus*, a thermophilic bacterium (22) (Dataset S6). The concordance of the outputs obtained with two different methodologies (and reference databases) reinforces our results.

Bacterial and Fungal taxa identified on the Turin Shroud

Overall sequencing data for bacterial, archaeal, and fungal biota, including the relative abundance of the phyla, classes, and orders, respectively, are summarized in Figure 2, with further details provided in the supplementary information (Datasets S4 and S5). Considering current knowledge of microbial ecology, the analysis of bacterial taxa associated with the TS samples revealed a notable presence of species commonly found on the human skin, particularly in sample AB1 and to a lesser extent in sample C3_ha. These include *Cutibacterium acnes* (formerly *Propionibacterium acnes*), *Staphylococcus epidermidis*, *Cutibacterium granulosum*, *Corynebacterium tuberculostearicum*, *Staphylococcus capitis*, and *Staphylococcus hominis* (23). Their presence indicates potential human skin contact with the analyzed samples.

Within the archaeal domain, the TS samples exhibited strong consistency in community composition, with most taxa recurring among the top entries. These predominantly belonged to the salt-tolerant class Halobacteria, which is adapted to high salinity environments. These findings suggest a pronounced overrepresentation of osmotically resilient species, which are typically associated with saline and drought-stressed conditions.

The fungal community displayed a significant abundance of *Debaryomyces hansenii*, a yeast species that thrives in dry and osmotically stressful environments (24), similar to the environments where the Turin Shroud was kept in the past. Saprophytic molds, such as *Aspergillus,* were also identified, along with fungi associated with human skin and scalp, particularly *Malassezia restricta*.

Taxonomic identification of a diverse array of bacterial, archaeal, and fungal taxa provided insight into the complex microbiome associated with the TS, shedding light on possible ecological and historical contexts. Bacterial profiles featured prominently skin-associated taxa, which indicate direct human contact, both in ancient and modern times. The high concentration of these bacteria in sample AB1, which is from a peripheral area likely exposed to environmental contamination, suggests frequent manipulation. Sample C/D12, taken from the hand region of the Shroud's image, further supports evidence of human contact. The detection of *Paraburkholderia* species, known for their ecological adaptability and occasional pathogenicity (25), may reflect broader environmental exposures over time.

Archaeal analysis revealed a consistent dominance of Halobacteria, which suggests an adaptation to saline environments. This could be related to ancient flax retting practices in brackish or salty water (26), which were more common than dew retting in antiquity (27). The dominance of *Debaryomyces hansenii* further supports salt tolerance and possible marine connections because the yeast is also found in seawater (24). The presence of *Aspergillus* points to possible degradation related to fluctuating storage conditions. The widespread presence of *Malassezia restricta*, a primary colonizer of the human skin (28), across all samples is a clear demonstration of ongoing human interaction with the Shroud.

Overall, the microbiological diversity of the Shroud samples offers valuable insight into its history. The recurrent presence of skin-associated bacteria and fungi implies direct contact with human beings, possibly during devotional religious ceremonies and cloth conservation treatments, in addition to the official sampling operations. These findings underscore the Shroud's dual significance as a religious relic and a historical artifact, reflecting both devotional and environmental influences throughout its existence.

Plant and Animal taxa identified on the Turin Shroud

A metagenomic assembly of the reads into contigs (see Material and Methods) and a nucleotide BLAST search enabled to extend the analysis to other kingdoms (Figure 3, and Dataset S7 and Dataset S8). In addition to *Homo sapiens*, our analysis of animal taxa revealed notable findings, particularly regarding the red coral (*Corallium rubrum*; 33.3%), a species endemic to the Mediterranean Sea (Figure 3B-C, and Dataset S7 and Dataset S8).

We extracted the reads showing patterns of deamination at their terminal bases from the animal and plant samples with more than 100 contigs, to evaluate signals of damage pattern, as in the human analysis (Figures S6 and S7).

We focused on the taxa whose identification was based on hits with at least 100 assigned contigs to avoid false positives, and found domestic cats and dogs to be

prevalent (21.7% and 22.1%, respectively), although DNA traces from several farm species, including chickens (*Gallus gallus domesticus*; 9,5%) and ruminants from the Bovidae family (cattle, goats, and sheep; 2,6% overall) were detected. Other livestock and wild animals such as pigs, horses, deer, and rabbits were also found. Weak traces of brown rats and mice suggest possible environmental contamination. Among the less abundant taxa identified (around 1% of assigned contigs), notable are some fish species including the gray mullet (*Chelon labrosus*), Atlantic cod (*Gadus morhua*), and ray-finned fishes (*Leuciscinae* spp.). Marine ostracods, particularly the small seafloor-dwelling crustacean *Notodromas monachal*, which is common in zooplankton communities, were also documented. Insects such as flies (Diptera), aphids (Hemiptera), and arachnids like dust and skin mites and ticks, including *Demodex folliculorum* and *Haplochthonius simplex*, were identified as well.

Plant taxa showed greater diversity (Figure 3D-E, and Dataset S7 and Dataset S8), with prominent species including carrot (*Daucus carota*; 30.9%) and bread wheat (*Triticum aestivum*; 11.6%), represented by more than 100 assigned contigs. Other cereals found encompassed durum wheat (*Triticum durum*), einkorn wheat (*Triticum monococcum*), maize (*Zea mays*) and rye (*Secale cereale*). Horticultural crops included peppers, tomatoes, and potatoes (Solanaceae), as well as melons or cucumbers (Cucurbitaceae). The Fabaceae family was also represented by a strong presence of peanuts (*Arachis* spp.), particularly in sample C/D12. Among forage species and their wild relatives, weak traces of perennial ryegrass, bluegrass, fescue, oats, and clovers were observed. The fruit trees identified with greater confidence included banana, almond, walnut, and sweet orange. Fainter DNA signals were detected for fig, pistachio, apple, pear, hazelnut, maple, and grapevine (*Vitis* spp.). The only non-cultivated plant with more than 100 assigned contigs was stinging nettle, but significant amounts of spruce trees and wild cardoons were also found (see Dataset S7 and Dataset S8).

The taxonomic identification of the plant and animal species on the Shroud reveals a complex biodiversity, albeit constrained by limitations in available reference databases. Reliance on a relatively small dataset (126 plant species and limited animal genomes) and the degraded condition of the DNA available made the taxonomic classification complicated. Nevertheless, several Viridiplantae taxa were confidently identified, particularly agricultural species such as carrots and cereals. Grouping of taxa at the genus level (*e.g.*, *Triticum*, *Aegilops*, *Hordeum*, and *Secale* spp.) reflects a parsimonious approach due to the overlapping of genetic signals. However, the strong signal for *Daucus carota* indicates that higher specificity could be obtained in some cases.

Among cultivated species, we also identified melon or cucumber, and various Solanaceae (tomato, pepper and potato). These reflect typical agricultural practices in the Mediterranean and other European territories. Fruit trees such as banana (*Musa acuminata*) and orange (*Citrus sinensis*) further highlight the diversity of cultivated plants possibly introduced through trade and indicate interconnected regional economies.

Non-cultivated species such as cardoon (*Cynara cardunculus*), maple (*Acer* spp.), spruce (*Picea* spp.), pine (*Pinus* spp.), nettle (*Urtica dioica*), and walnut (*Juglans* spp.) reflect local ecological diversity. Notably, cardoon and nettle are indigenous to Europe and the Mediterranean area. Wild cardoon remains widespread in southern Europe and North Africa, and it was domesticated in the western Mediterranean (29, 30). Stinging nettle, native to Europe and widely distributed across Asia and North Africa, is valued both as a vegetable and in traditional Indian medicine (31). The uncertain origin of melon is also noted, with hypotheses pointing to ancient Persia or Africa (32).

Although none of the identified plant taxa can be uniquely associated with the Levant and the Middle East, several genera originated in the Fertile Crescent and are now widespread across the Mediterranean Basin. For example, almond trees, pistachios, and figs are native to and have been domesticated in the Near or Middle Eastern areas (33–35), following the introduction by Romans to Southern Europe and Northern Africa during the first centuries CE.

The presence of exotic species introduced to Europe from Central and Eastern Asia, and North and South America, was also noted. Maples, for instance, are thought to have originated in Asia, with genetic studies suggesting that the genus *Acer* likely emerged in East Asia, particularly in China. However, fossil evidence indicates that some species may have evolved independently in North America (36). Bananas, whose secondary center of diversification is Africa, were introduced to Europe by Portuguese sailors in the early sixteenth century, but they gained popularity only by the eighteenth century. This shift was driven by improved agricultural practices and trade networks, including plantation systems in Central America (*e.g.*, the Caribbean), which helped establish bananas as a staple fruit in Europe (37).

Several plant taxa identified here, such as *Picea abies*, *Juglans regia*, *Pinus* spp. *Cucumis* spp., *Cichorium* spp., *Cynara* spp., and *Vitis* spp., were also found in previous palynological and/or molecular studies (9, 38–40). These findings support a view of the Shroud as being associated with a blend of local vegetation and historical agricultural practices.

Animal taxa presented a more complex identification challenge due to the genetic similarities among related species. The presence of *Corallium rubrum* underscores the region's historical reliance on marine resources. This endemic Mediterranean red coral has been known since the time of the Roman Empire and held considerable cultural, economic, and symbolic significance in antiquity. It was primarily fashioned into jewelry, amulets, talismans, and decorative objects. Several ancient texts from the Middle Ages attest to its use in medical contexts, as it was believed to possess healing properties and was utilized in remedies for various ailments and disorders. Regarded as a valuable commodity, red coral was transported for centuries along Mediterranean trade routes, facilitating economic and cultural exchanges among populations and regions. The trade of red coral saw further development during the medieval period, particularly in Mediterranean ports (41, 42).

Livestock species as well as cats and dogs, reflect long-standing agricultural and domestication practices in local farms and rural settings. The presence of mites and ostracods, including the abundant *Notodromas monacha*, which are very common in terrestrial and aquatic habitats illustrates the ecological diversity and may reflect environmental conditions during the storage or handling of the Shroud.

Genetic affinities among the Turin Shroud samples

To highlight potential similarities among the TS samples, we performed two different analyses based on their metagenomic profiles. The artificially contaminated linen fragment was used as an outgroup.

The Principal Component Analysis (PCA) revealed the outlier behavior of AB1, which represents the TS later edge, while samples derived from the areas of face, hands, gluteal region, and feet of the body image of the Man of the Shroud did not show distinct patterns related to sampling type (linen fragment vs. vacuum dust) (Figure 4A). On the other hand, C12_fe and R58, collected from the Shroud and the Reliquary, respectively, were the samples with the highest number of private taxa in the hierarchical clustering plot (Figure 4B). It is important to note that the outgroup used as control was confirmed as outlier by both analyses and its genetic differentiation from each of the TS samples was comparable. In addition, although the first two components accounted for about 72% of the overall genetic variation, most TS samples were closely clustered by PCA, except for AB1. This low discrimination is partially due to the method, which could obscure differences between samples (see Materials and Methods). However, a closer examination of the overall genetic data (Dataset S7) reveals the presence of both different and similar organisms among the pairwise comparisons of the TS samples. These include several domesticated species, such as cereals, vegetables, pets, and farm animals. We believe that this commonality can be explained by two hypotheses rather than solely by the sample history. The first hypothesis is technical: these species are well-described and included in various databases, thus any misalignment during identification is likely to occur with higher frequency. The other hypothesis calls for secondary contamination, which refers to DNA traces resulting not from the direct exposure of the TS samples to those particular species, but rather from human contact with those organisms. Basically, we could hypothesize the presence of a sort of secondary metagenomic fingerprint. This would lead to a collection of species that appear with greater probability than others. However, this hypothesis could not be explored further within our project because it would require a comparison of additional samples (similar to the TS) from different origins.

The presence of recurrent species, while potentially introducing background noise, must be emphasized: numerous other species were identified exclusively in specific samples of the Shroud or with exceptional clarity, such as *Daucus carota* and *Corallum rubrum*.

Reappraisal of the overall biodiversity found on the Turin Shroud

The study aimed to isolate and characterize genomic DNA sequences from the available original official samples of the Turin Shroud collected in 1978 by Prof.

Pierluigi Baima Bollone from various sections of this linen cloth. Its final goal was to identify the biological sources of environmental contaminants—including pollen, plant fibers, fungal structures, animal hairs, blood residues, and human biological fluids—found in linen filaments, a vacuum dust sample, and a small cloth fragment. Our new findings, alongside previous ones (9), confirm the presence of plant and animal DNA, as well as traces of DNA from various human subjects on the Shroud of Turin. The identification of diverse DNA sources provided insights into potential connections between the temporal and geographic pathways related to hypotheses on the Shroud's origin. Many identified plant species are native to and widespread in Central Europe and the Mediterranean Basin, extending from the Iberian Peninsula to the Middle East.

The most prominent crop identified in the TS samples is carrot (30.9%). Both historical records and molecular analyses suggest that carrots, characterized by purple and yellow roots, were domesticated in Central and Minor Asia, and then introduced to Western Europe (43–45). It is worth mentioning that out of approximately 3,800 contigs, about half were confidently mapped to unique sites of the carrot genome, whereas the remaining half mapped to multiple locations being likely associated with repetitive sequences. The majority of the contigs originated from the C10 sample, comprising 1,787 contigs (94.4%), whereas only 2 and 1 contigs are from AB1 and B12 samples, respectively. SNPs common to a DNA sequence dataset of carrot accessions (46) belonging to five distinct populations were employed to calculate their similarity. Based on this analysis, carrot DNA contaminations found on the Shroud were shown to be genetically more similar to improved cultivars and early cultivars (Figure 5), which are descendants of orange carrots developed in Western Europe between the 15th and 16th centuries (47). These genetic signatures suggest a relatively recent contamination – not before the late Middle Ages – due to carrot residuals most likely associated to plant materials of Western European origin.

Another abundant crop among those identified in the TS samples is wheat and its close relatives. All cultivated polyploid forms originated and were domesticated in the Fertile Crescent and were subsequently introduced in the Mediterranean Basin from the Middle East. By the 1st century BC, with the emerging Roman Empire, wheat had become well-established in the region and recognized as an essential agricultural commodity. Additionally, the presence of exotic species introduced to Europe from Central and South-Eastern Asia, and North and South America, was noted. For example, maples, oranges and bananas were identified. Maples are thought to have originated in Eastern Asia, despite some evidence suggesting a North American origin (36). Moreover, oranges, which are originally from the region encompassing Southern China and North-Eastern India, and bananas, whose earliest evidence of domestication is Papua New Guinea, were introduced to the Mediterranean Basin by the Muslim conquerors and Portuguese sailors, respectively, between the 9th and 10th centuries and 15th and 16th centuries (37, 47). The identification of animal taxa posed a more intricate challenge owing to genetic similarities among closely related species (*i.e*. members of the Bovidae family). The presence of both wild and farm animals, including several livestock

species and pets, indicates the enduring nature of agricultural and domestic practices prevalent in rural settings. The diversity of animals and plants at multiple taxonomic levels suggests that much of the environmental Shroud's contamination occurred in recent centuries, particularly after the voyages of Marco Polo and Christopher Columbus. This hypothesis is consistent with and further corroborates our previous findings (3, 9).

In this study, we also identified human mitochondrial variants, which can be classified into one main haplogroup (K1a1b1a, which is the same of the collector), and those with diagnostic motifs of different lineages, such as H1b, an ancient late glacial marker common in Western Eurasia, and H33, which is typical of the Near East and particularly frequent among the Druze (17) as previously documented by Barcaccia *et al*. (9). Notably, the Druze population shares a common genetic ancestry with Jews and Cypriots, and has historically intermingled with other Levantine populations, including Palestinians and Syrians (16, 17). Although additional single nucleotide polymorphisms (SNPs) were identified, it was not possible to reconstruct complete mitogenome haplotypes that could be confidently classified into any of the South Asian minor lineages (e.g., M39, M56, R7, and R8) identified in our previous study by analyzing mtDNA hypervariable segment I (HVS-I) from a different sample of the Shroud of Turin (9). In that study, over 55.6% of the human mtDNA HVS-I reads were classified into Near Eastern lineages, while Western European lineages accounted for less than 5.6%. The presence of approximately 38.7% of Indian ethnic lineages could have resulted from historical interactions or the Romans importing linen from regions near the Indus Valley, associated with the term "Hindoyin" found in rabbinic texts (10). Notably, the term "Shroud", derived from the Greek "Sindôn" meaning fine linen, may be related to Sindh, a region renowned for its high-quality textiles. Historical evidence supports trade links between India and the Mediterranean, underscoring the significance of these textiles and inviting further exploration of ancient cultural interactions and trade practices. Indeed, the biblical scholar Levergne stated that the term "Sindôn" refers to a fabric of Indian origin, valued for its qualities and used for various and multiple purposes (48). In brief, a reappraisal of those outcomes from the analysis of the DNA traces found on the Shroud of Turin suggests the potentially extensive exposure of the cloth in the Mediterranean region and the possibility that the yarn was produced in India.

Overall, our prior and present findings provide valuable insights into the geographic origins of individuals who interacted with the Shroud throughout its historical journey across various regions, populations, and eras.

Conclusions

In this study, we sequenced and characterized genomic DNA traces extracted from the cloth edges, previously used for radiocarbon dating, and from other sections bearing the image of the Man of the Shroud. Molecular traces of contamination from individuals who handled the Shroud with limited protective precautions, including the 1978 sampling team in Turin, were expected. Our analysis revealed that the predominant mitochondrial lineage is characteristic of Ashkenazi Jews and

matches the mtDNA haplotype (and genomic data) of Prof. Baima Bollone, the collector, as also confirmed by kinship analyses on the entire genome. Diagnostic variants of other haplogroups, such as H33 found in Middle Eastern populations (*i.e*. Druze), were also detected, alongside the Western Eurasian haplogroups H2a2 and H1b. The occurrence of an unusually high number of human heteroplasmies and the coexistence of different mtDNA variants confirm that the Shroud came into contact with multiple individuals, thereby challenging the possibility of identifying the original DNA of the Shroud.

Intense human handling is confirmed by skin bacteria such as *Cutibacterium* and *Staphylococcus*. Halophilic archaea indicate salt preservation or saline storage conditions, but the presence of *Debaryomyces hansenii* and other fungi found in cheeses and hyper-saline waters raises further questions. Concerning the Shroud's journey, the presence of red coral, livestock (*e.g*. chickens, cows, pigs, goats, sheep, rabbits, horses), and domestic cats and dogs suggest Mediterranean origins or transit through Mediterranean regions.

Plant DNA analyses revealed the predominance of cultivated species, which has historical implications. The concomitant and very abundant presence of both *Daucus carota* (domesticated carrot) and various *Triticum* species (cultivated wheat) suggests agricultural practices with both native and introduced crops. Carrot is the most prominent crop plant species identified in the Shroud. Wild populations of carrots with white roots have existed in Europe since more than two thousand years, as they were described by Pliny the Elder in the encyclopedic "Naturalis Historia" and used by Romans for medicinal purposes and food preparations (see Apicius, "De re culinaria" a collection of Roman cookery recipes). However, we demonstrated that the carrot DNA found on the Shroud is genetically more similar to early cultivars and improved cultivars, which were proven to descend from orange carrot varieties developed in Europe between the 15th and 16th centuries (46). Furthermore, oranges and bananas, which are originally from Southern Asia and Eastern Oceania (China and Papua New Guinea), were introduced to the Mediterranean Basin by Muslim populations and Portuguese sailors in the high-late Middle Ages (37, 47). Post-Columbus species, such as maize (domesticated in Mexico), Solanaceae crops (*e.g*. tomatoes, peppers, and potatoes), and peanuts (Fabaceae), which are crop plants native to Latin America, pose an additional significant conundrum about the antiquity of the Shroud, even if a later contamination cannot be ruled out. DNA traces from various species and regions, including the Middle East, Mediterranean, Europe, America and Asia, indicate that the Shroud was exposed to different environments and peoples. The prevalence of Mediterranean crops and the absence of typical Middle Eastern flora raise questions about the agricultural landscape when the Shroud was created or used as a burial cloth. Comparative analyses with other ancient textiles and artifacts could further illuminate cultural and historical interactions with plants and animals.

In conclusion, genetic and microbial evidence discloses a complex history of the Turin Shroud, reflecting interactions with a diverse array of individuals and exposure to various agricultural and environmental contexts. While some human

mtDNA haplogroups may correspond to those who handled and sampled the historical artifact, the overall DNA results – derived from rigorous methodological handling in clean rooms and metagenomic analyses supported by robust bioinformatics – suggest a diverse mosaic of genetic traces. The age of the Turin Shroud cannot be determined through metagenomics because this methodology is unable to provide any robust evidence supporting either a Medieval origin or a history dating back two millennia. Nevertheless, our findings constitute a novel and significant contribution to the field, thoroughly elucidating the biological traces left by centuries of social, cultural, and ecological engagement. Furthermore, the radiocarbon dates of two distinct fabric threads collected from the reliquary confirm their use in mending and patching efforts aimed at stabilizing the fire-damaged linen cloth during two well-documented events in 1534 and 1694 CE. Collectively, our findings illuminate important aspects of the Shroud's preservation history.

Addendum

In memory of Dr. Pierluigi Baima Bollone, coauthor of this publication, whose sudden departure has left our research groups at a loss for words.

As Pierluigi Baima Bollone passed away in Turin, Italy, on November 5, 2025, we wish to express our profound gratitude for his irreplaceable collaboration, invaluable contribution and unwavering dedication to the advancement of knowledge regarding the Turin Shroud.

Bibliographical notes: Pierluigi Baima Bollone was a prominent medical doctor specialized in hematopathology and a full professor of forensic medicine at the University of Turin. He founded and led the Department of Diagnosis and Prevention at Gradenigo Hospital. A prolific author of scientific publications, dissemination books and forensic medicine manuals, his works are widely adopted in academia. Renowned on both national and international stages, he produced influential writings in criminology and forensic medicine. He also served as Honorary President of the International Centre for Sindonology in Turin, the official institution devoted to the study of the Shroud, contributing extensively to its literature.

646 # Materials and Methods

647 ## Sample collection

648 For the present study, twelve samples were retrieved from the 1978 Turin Shroud
649 collection (Table 1 and Figure S1): seven glass tubes with linen cloth filaments,
650 four jars with vacuum dust (one completely empty), and one microscope slide with
651 a tiny biological fragment. This collection is entirely new compared to the one
652 analyzed in Barcaccia *et al*., 2015 (9).
653

654 ## Sequence data production

655 DNA was extracted from all available samples using a silica-based technique that
656 allows for recovery of ancient/historical DNA even when molecules are very few
657 and highly fragmented, as in (49). After DNA extraction, DNA concentration and
658 fragmentation were assessed by fluorometer and capillary electrophoresis,
659 respectively. For samples with a DNA concentration higher than zero, shotgun
660 genomic libraries were constructed following a custom double indexing protocol
661 optimized for ancient DNA using partial uracil DNA glycosylase treatments (half-
662 UDG), which partially retain the deaminated cytosines resulting from DNA damage
663 (50).
664 Considering that 10M reads are required for an accurate estimation of the
665 endogenous content, the half-UDG genome libraries were multiplexed and
666 sequenced on the Illumina platforms (NextSeq 550 and 2000) using a paired-end
667 strategy. A present-day filament of linen was artificially contaminated by one of the
668 handlers (operator) to validate the feasibility of our approach.
669 The modern DNA of the collector (Prof. Baima Bollone) was also extracted using
670 the Maxwell® RSC Stabilized Saliva DNA Kit after collecting a biological sample
671 with the IsoHelix GeneFiX™ Saliva DNA Collection Kit. For this modern sample, a
672 genomic library was prepared with the Illumina DNA Prep Kit using the standard
673 protocol and sequenced on the Illumina NextSeq 2000.
674

675 ## Sequence data analyses

676 The raw shotgun sequence data have been demultiplexed using bcl-convert v.
677 00.000.000.4.2.4 (51). Raw fastq and adapter trimming have been performed
678 using AdapterRemoval v. 2.3.2 (52), discarding reads shorter than 30 bases after
679 trimming and collapsing paired-end reads overlapping by at least 11 bases
680 (parameters: *–trimns –maxns 2 –trimqualities –minquality 2 –minlength 30 –*
681 *collapse –minalignmentlength 11*). Trimmed reads were mapped to the human
682 reference genome hs37d5 using bwa v. 0.7.17-r1188 (53) with the aln/samse
683 algorithms and parameters (*-l 1024 -n 0.01 -o 2*) optimized for ancient DNA (54).
684 After mapping, aligned reads were filtered for a minimum mapping quality of 20
685 and duplicates were removed using samtools v. 1.17 (55) and DeDup v. 0.12.8
686 (56), respectively. The two terminal bases of each read in the final BAM files were
687 soft-clipped using trimBam from BamUtil v. 1.0.15 (57), to mask potential aDNA
688 damage patterns for downstream analyses. Statistics and aDNA damage patterns
689 were evaluated with QualiMap v.2.2.2-dev (*bamqc*) (58) and mapDamage v. 2.1.0

690 (59). Genetic sex was evaluated following the two methods described in Skoglund
691 *et al*. (60) and and Mittnik *et al*. (61). For the mtDNA, the trimmed reads were
692 aligned to a modified version of the rCRS (62), obtained using CircularGenerator
693 v. 1.0 from CircularMapper (63), with bwa aln/samse and the same parameters as
694 indicated above. RealignSAMFile v. 1.0 (from CircularMapper) was used to realign
695 the reads to the original rCRS. BAM files were filtered in the same way as above.
696 Mitochondrial DNA haplogroups were called using Haplocheck v. 1.3.2 with default
697 options (64).
698 For a reliable haplogroup classification, ANGSD v 0.940-dirty (65) was also used
699 to call a consensus mitochondrial sequence with the following parameters: *-minQ*
700 *20 -setMinDepth 2 -minMapQ 30 -doFasta 2 -doCounts 1 -basesperLine 60*.
701 Consensus files were uploaded on HaploGrep v 3.2.1 (66). The mitogenome data
702 were also analyzed with Haplocheck v. 1.3.2 (64), which was also used to
703 construct schematic phylogenetic trees.
704

705 ## Contamination estimate

706 Contamination estimate on the mtDNA was obtained using contamMix v. 1.0-10
707 (67). A consensus sequence from the aligned mtDNA reads was called with
708 ANGSD v. 0.940-dirty (65) using the following parameters: *--minMapQ 30 -minQ*
709 *20 -doCounts 1 -setMinDepth 3 -doFasta 2*. The original mt-aligned reads were
710 mapped to this consensus and used, together with a database containing 311
711 worldwide mitochondrial genomes, plus the consensus generated with ANGSD, to
712 estimate potential mt contamination with contamMix (parameters: *–nIter 50000 –*
713 *nChains 3 –trimBases 2*). Nuclear contamination was estimated using hapConX
714 (68) for those samples classified as male individuals.
715 PMDtools (13) was used to assign PMD score to all reads mapped to the human
716 genome and to extract endogenous ancient DNA sequences, separating them
717 from contaminating modern sequences using postmortem degradation patterns.
718

719 ## Modern reference individual

720 The raw reads from the modern reference individual were processed using fastp
721 v. 0.24.0 (69) with parameters *-g -x -c*. Trimmed reads were mapped to the hs37d5
722 human reference using bwa-mem2 (70). Duplicates were removed using picard-
723 tools MarkDuplicates (71) and final statistics were calculated using mosdepth v.
724 0.3.6 with default parameters (72).
725

726 ## Kinship analysis

727 Kinship analyses were performed using the samples showing a sufficient average
728 depth of coverage on the human genome, together with the modern reference
729 individual. Three different analyses were performed using READ v. 2 (73) and
730 BREADR (74) and KIN (75). PileupCaller (from sequenceTools v. 1.5.3.2) (76) was
731 used to call pseudohaploid genotype data on the 1240K SNPs set to be used as
732 input data for READ2 and BREADR.
733

Proteomics methods

Three TS samples (C/D12, B12, and R58) were extracted by adding 5% SDS / 50 mM TEAB buffer (20 µL to samples B12 and C/D12 and to two negative controls; 30 µL to R58). Extraction proceeded by alternating 30 min in a sonicator at 56 °C with 30 min on a thermomixer hotplate at 1,600 rpm, repeated over 5 h. Samples and negatives were then incubated overnight at 56 °C without shaking. The following day, five 1.4 mm ceramic beads, pre-cleaned with bleach, rinsed with methanol, and UV-irradiated overnight, were added to each tube. Mechanical homogenization was performed using a Precellys tissue lyser at 6,500 rpm for 30 s. Lysates were centrifuged at 12,700 rpm (max speed) and supernatants transferred to protein low-bind tubes. For each sample, a final volume of 23 µL was prepared (adding extraction buffer as needed) for downstream S-Trap processing. Reduction was carried out by adding 1 µL of 60 mM DTT and incubating at 55 °C for 15 min. Alkylation followed by adding iodoacetamide (IAM) to a final concentration of 500 mM stock solution, incubating in the dark for 30 min at room temperature. Excess IAM was quenched by adding 1 µL DTT. To acidify the solution, 2.6 µL of 27.5% phosphoric acid was added, followed by 165 µL of S-Trap binding buffer consisting of 100 mM TEAB in 90% methanol. Acidified samples were loaded onto S-Trap micro spin columns and centrifuged at 4,000 ×g for 30 s. Each column was washed three times with 150 µL of binding buffer. Digestion was performed by adding 0.5 µg sequencing-grade trypsin in 50 mM TEAB directly onto the columns, followed by incubation for 2 h at 47 °C.

Peptides were eluted following the standard three-step S-Trap elution protocol: 40 µL of 50 mM TEAB, 40 µL of 0.2% formic acid in water and 40 µL of 50% acetonitrile / 0.2% formic acid. Each elution step included centrifugation at 4,000 ×g for 30 s, and eluates were pooled. Peptide solutions were dried overnight in a fume hood prior to MS analysis.

Peptide samples were analyzed by liquid chromatography–tandem mass spectrometry (LC–MS/MS) using a Thermo Scientific Orbitrap Astral mass spectrometer coupled to a Thermo Scientific Neo nano-UHPLC system via a nano-electrospray ionization source. Peptides were separated on a reversed-phase C18 analytical column (75 µm internal diameter, 25 cm length) operated at a nominal flow rate of 300 nL/min. Mobile phase A consisted of water and mobile phase B of acetonitrile, both containing 0.1% formic acid. Peptides were eluted using a linear gradient from 1% to 55% solvent B over 45 min, followed by a column wash at 99% B and re-equilibration, for a total run time of 52 min.

The mass spectrometer was operated in positive ion mode. Full MS survey scans were acquired in the Orbitrap analyzer over an m/z range of 350–1500 at a resolution of 240,000. Data-dependent MS/MS acquisition was performed with precursor ions selected for fragmentation using an isolation window of 1.5 m/z. Fragment ions were acquired in the Astral analyzer over an m/z range of 150–1800 using higher-energy collisional dissociation (HCD). Dynamic exclusion was enabled to minimize repeated sequencing of the same precursor ions. All other instrument parameters were set according to manufacturer recommendations and are reported in the supplementary methods.

779 The raw data were analyzed using Progenesis QI for Proteomics version 4.2.
780 Specifically, one experiment was conducted on the three samples only, and one
781 separate experiment was conducted on the two negative controls, to identify
782 proteins present in either the samples or in the negatives. After importing the data,
783 all samples aligned against the selected reference with a similarity score greater
784 than 90%. Peptide ions with charge 2-5 were kept, together with those with more
785 than 2 isotopes. Overall, 3900 peptide ions were retained for the “samples” group,
786 and 1359 for the “negatives” group. Peptides with a ranking 1-3 were exported in
787 Mascot for identification. Search parameters were the following: semiTrypsin
788 searches, with 2 missed cleavages allowed, fixed modification Carbamidomethyl
789 (C) and variable modifications Deamidation (NQ) and Oxidation (M), peptide mass
790 tolerance 10 ppm, fragment mass tolerance 0.02 Da, target FDR 1%. Results were
791 further refined using Percolator. Peptide identified with a score smaller than 7 (for
792 “samples”) and 12 (for “negatives”) were excluded from further analyses (as per
793 Mascot peptide score distribution to indicate identity or extensive homology), as
794 well as proteins identified by less than 2 unique peptides.
795

796 ## Taxonomic classification of the DNA sequences

797 The sequenced reads from the seven samples that underwent metagenomic
798 analyses (Table 1) were processed to trim adapters and filter for quality using Trim
799 Galore v0.6.7 (77). Initial taxonomic classification of the reads was performed
800 using Kraken v2.1.2 (78) with default parameters for paired-end library reads. The
801 database used was a combination of pre-built Kraken databases, named archaea,
802 bacteria, plasmids, human, fungi, viruses, protozoa, and plants. An interactive
803 visualization of the results, known as a Krona graph, was generated from the
804 textual Kraken reports using KrakenTools (see Supplementary information,
805 including Dataset S5) (79).
806 An additional classification of the reads, applicable only to microorganisms, was
807 performed using the MetaPhlAn program (21). All reads assigned by Kraken to a
808 taxon ID belonging to Archaea, Bacteria, or Fungi, or not assigned to any taxa,
809 were extracted using TaxonKit v0.18.0 (80), SeqKit v2.1.0 (81), and a custom awk
810 command. The resulting paired-end FASTQ files were analyzed with MetaPhlAn
811 v4.2.2 using the default settings, except for the parameter -t, which was set to
812 "rel_ab_w_read_stats".
813 Due to the absence of Metazoa records (except for *Homo sapiens*) in the Kraken
814 database and the small number of Viridiplantae species included, Kraken2
815 analysis is not suitable for accurately identifying reads from these kingdoms.
816 Therefore, a different approach was chosen. Raw reads were assembled into
817 contigs for each sample using Megahit v1.2.9 (82) with the parameters --presets
818 meta-large and --min-contig-len 100. Taxonomic classification of the resulting
819 contigs was conducted using BLASTn v2.12.0 (83) against the entire NCBI nt
820 database (84), downloaded on December 6, 2024. The alignment parameters
821 were: -evalue 1e-5, -max_target_seqs 5, -perc_identity 90, and -outfmt 6. The
822 parameters qcov, qcovhsp, and staxids, were added to the standard fields for
823 subsequent filtering and processing.

824 A preliminary filtering of the alignment results was performed to generate summary
825 statistics. Alignments with query coverage below 90% were excluded, and for each
826 contig, the best target based on E-value was selected. A custom Bash and
827 Python3 script, utilizing TaxonKit v0.18.0 (80), was used to calculate the number
828 of contigs assigned to different taxa at each taxonomic rank.
829 The tabular output of the BLASTn alignments was further processed for taxonomic
830 classification. For each contig, alignments with query coverage below 90% were
831 excluded. Remaining alignments were compared based on their highest-scoring
832 HSP (high-scoring pair) for each target. This comparison aimed to determine
833 whether the alignments were of similar significance. Alignments were deemed non-
834 equivalent if any of the following criteria were not met: a maximum difference in
835 percent query coverage of 3, a maximum difference percent identity of 3, a
836 maximum difference in bit score of 10%, a maximum difference in E-value of three
837 orders of magnitude. If one alignment outperformed all others, the contig was
838 assigned to the corresponding taxonomic ID (taxid). If two or more alignments were
839 equally probable, the contig was assigned to the lowest taxonomic node present
840 in the genealogy of all target taxid. Contigs assigned to taxa above the family rank
841 were discarded as too unspecific. This processing was implemented using a
842 custom Bash and R script, incorporating TaxonKit (80) and the R package rentrez
843 v1.2.3 (85). All custom scripts are available upon request.
844 A final step was implemented to filter potential false positives. A manual
845 interpretation of the tables containing all contigs assigned to a taxon was
846 necessary to eliminate possible false positives. Two criteria were established: i)
847 When multiple species within the same genus produced similar hits, or if the
848 number of contigs assigned to the genus exceeded that of contigs assigned to any
849 individual species within it, the contigs were assigned to an unidentified species
850 within that genus (*e.g.*, *Musa* spp.); ii) In cases where a substantial number of
851 contigs identified a specific species, as well as the corresponding genus, subtribe,
852 and tribe, all contigs were assigned to the species (*e.g.*, *Daucus carota*). These
853 reads likely represent broader, less specific regions that remain associated with
854 the species, and it is prudent to accurately specify and categorize them
855 accordingly.
856 This methodology was developed in response to findings related to monkeys,
857 which likely yielded results associated with human DNA. Given our confidence
858 regarding the presence of human DNA, it is highly improbable that various exotic
859 monkey DNAs are present. We anticipate that in other instances, a small number
860 of contigs will also identify species related to the primary target. This phenomenon
861 may arise from the short contigs generated from degraded sequences, which can
862 align, albeit infrequently, to incorrect targets when conserved regions are present.
863

864 Clustering of the samples

865 The analysis conducted on the seven samples was also applied to the modern
866 reference individual (hereafter referred to as "control"), with minor variations in the
867 steps involving Fastp, Megahit, and Kraken2. The same parameters were utilized,

868 except for the use of single-end mode instead of paired-end mode, which was
869 dictated by the sample's nature.
870 To elucidate the differences among the samples, it was imperative to select a
871 taxonomic rank that would minimize potential assignment errors between species
872 or genera, thereby ensuring that reads assigned to that taxon could be regarded
873 as accurate and reliable. The variation in classification practices across different
874 kingdoms necessitated the choice of distinct taxonomic ranks corresponding to
875 each kingdom: Archaea at the class level, Bacteria at the phylum level, and
876 Metazoa and Fungi at the order level, while Viridiplantae was classified at the
877 family level.
878 A matrix was constructed to display the number of contigs assigned to each
879 defined taxonomic unit across the seven samples and the control. Subsequently,
880 a principal component analysis (PCA) was performed using the R function
881 "prcomp", with the parameter scale = TRUE to prevent the Primates order from
882 disproportionately influencing the variability. This clustering effectively represents
883 the variance among the samples. However, it has the potential to overemphasize
884 the significance of taxa represented by only a single contig in any given sample.
885 To mitigate this issue, a second clustering analysis was conducted, wherein all
886 taxa with a total number of contigs less than or equal to three were excluded. The
887 number of contigs for each sample was then normalized by dividing each value by
888 the maximum observed value, effectively rescaling all values to a range of 0 to 1
889 (max normalization by columns). This was followed by a row-wise max
890 normalization to ensure that every taxon held equal weight in the analysis. Finally,
891 the Euclidean distances between samples were calculated and subjected to
892 hierarchical clustering using the R functions from the pheatmap package (86).
893

894 ### Genetic ancestry of carrot DNA contamination

895 To determine the genetic ancestry of the carrot DNA found on the Shroud, a
896 comparative genomic analysis was performed against the *Daucus carota*
897 reference genome (46). Contigs from Shroud samples R58, AB1, B12, C10_gl,
898 and C/D12 — identified as *D. carota* — were mapped independently to the
899 reference genome. In parallel, Illumina reads (~10x) from 200 diverse carrot
900 samples were aligned to the reference, and SNPs were identified using the GATK
901 (Genome Analysis Toolkit) pipeline (87). The carrot samples represented five
902 distinct populations as defined by Coe et al. (46): Early cultivars, Improved
903 cultivars, Landrace A, Landrace B, and Wild. For each population, 40 accessions
904 with an ancestry coefficient >0.7 were selected. Both early and improved cultivars
905 represent lineages descended from carrot cultivars developed in the 15th and 16th
906 centuries. Landrace A and Landrace B consist of descendants from
907 Central/Eastern Asia and Western/Southern Asia, respectively, exhibiting semi-
908 domesticated phenotypes. Wild accessions represent undomesticated carrots
909 from Europe. Because samples R58, AB1, B12, and C/D12 yielded <3 uniquely
910 mapped contigs, they were excluded from further analysis. In contrast, sample
911 C10_gl provided 1,787 uniquely mapped contigs and was used for all downstream
912 analyses.

To estimate genetic similarity, Identical by State (IBS) counts were calculated using the overlapping SNPs between the carrot accessions and the C10_gl contigs. To ensure the reliability of the analysis and account for potential biases in contig distribution, a subsampling approach was employed: twenty contigs were randomly selected from the 1,787 available for C10_gl, with this process repeated for 100 iterations. The resulting non-IBS percentages were analyzed using t-tests and linear models in R (88) to determine if the genetic distances between C10_gl and the known phylogenetic groups were statistically significant. In this framework, lower non-IBS percentages denote higher genetic similarity, indicating a closer ancestral relationship. Plots were generated in R using ggplot2 (89).

Acknowledgments

The authors wish to express their gratitude to Emanuela Marinelli, an internationally recognized scholar of the Shroud of Turin, for her valuable insights and constructive comments on the sindonological aspects, particularly during the initial phase of research planning and the final phase of discussing the overall findings. Her support made this project possible and greatly enriched our work. We would also like to thank Alberto Cenzato, who assisted us in revising the Kraken code and managing the resources necessary to run it. We are deeply grateful for his work and dedication, which enabled us to overcome this technical challenge.

This study was funded by the Italian Ministry for Universities and Research (MUR) PRIN 2022 grant 2022Y8BSAL (A.A.); Fondazione Cariplo—Bando Giovani Ricercatori 2023, rif: 2023–1373 (N.R.M.); University of Padova (UNIPD), BIRD 2025, project A metagenomic survey of the linen cloth samples officially collected from the Turin Shroud in 1978, DAFNAE1–DOR–00719 (G.B.). UKRI FLF grant n. MR/Y019989/1 (N.P.). We acknowledge the CINECA award under the ISCRA initiative, for the availability of high-performance computing resources and support.

Data availability

Genomic sequences (raw data in FASTQ format) have been deposited in the European Nucleotide Archive (ENA; https://www.ebi.ac.uk/ena/browser/home) under the accession number PRJEB88938. Any additional information required to reanalyze the data reported in this paper is available from the lead contacts upon request.

References

1. E. J. Jumper, *et al.*, “A comprehensive examination of the various stains and images on the Shroud of Turin” in *Archaeological Chemistry—III*, Advances in Chemistry., (American Chemical Society, 1984), pp. 447–476.

2. A. Adler, *The orphaned manuscript - a gathering of publications on the Shroud of Turin* (Effatà Editrice, 2014).

3. W. Meacham, *et al.*, The Authentication of the Turin Shroud: An Issue in Archaeological Epistemology [and Comments and Reply]. *Current Anthropology* **24**, 283–311 (1983).

4. M. Antonacci, *The resurrection of the Shroud: new scientific, medical, and archeological evidence* (Evans & Co., 2000).

5. G. Fanti, R. Basso, *The Turin Shroud: Optical Research in the Past, Present and Future* (ITA, 2008).

6. E. Poulle, Les Sources de l’Histoire du Linceul de Turin. Revue Critique. *Revue D?Histoire Ecclésiastique* **104**, 747–782 (2009).

7. P. E. Damon, *et al.*, Radiocarbon dating of the Shroud of Turin. *Nature* **337**, 611–615 (1989).

8. T. Casabianca, E. Marinelli, G. Pernagallo, B. Torrisi, Radiocarbon dating of the Turin Shroud: new evidence from raw data. *Archaeometry* **61**, 1223–1231 (2019).

9. G. Barcaccia, G. Galla, A. Achilli, A. Olivieri, A. Torroni, Uncovering the sources of DNA found on the Turin Shroud. *Sci Rep* **5**, 14484 (2015).

10. A. Grossi, Jewish shrouds and funerary customs: a comparison with the Shroud of Turin in (Centro Español de Sindonologia (CES), 2012), pp. 1–33.

11. G. Riggi di Numana, *Rapporto Sindone (1978/1987) - Cronache e commenti dei fatti accaduti dal 1978 al 1987 intorno alle ricerche scientifiche condotte sulla Sacra Sindone di Torino* (3M Edizioni, 1988).

12. The 1978 Scientific Examination. Available at: https://www.shroud.com/78exam.htm [Accessed 11 November 2025].

13. P. Skoglund, *et al.*, Separating endogenous ancient DNA from modern day contamination in a Siberian Neandertal. *Proceedings of the National Academy of Sciences* **111**, 2229–2234 (2014).

14. M. D. Costa, *et al.*, A substantial prehistoric European ancestry amongst Ashkenazi maternal lineages. *Nat Commun* **4**, 2543 (2013).

15. I. Cardinali, *et al.*, Mitochondrial DNA footprints from Western Eurasia in modern Mongolia. *Front. Genet.* **12**, 819337 (2021).

16. D. M. Behar, *et al.*, The genome-wide structure of the Jewish people. *Nature* **466**, 238–242 (2010).

17. L. I. Shlush, *et al.*, The Druze: A Population Genetic Refugium of the Near East. *PLOS ONE* **3**, e2105 (2008).

18. A. Modi, *et al.*, Paleogenetic and morphometric analysis of a Mesolithic individual from Grotta d'Oriente: An oldest genetic legacy for the first modern humans in Sicily. *Quaternary Science Reviews* **248**, 106603 (2020).

19. A. Nicolotti, *The Shroud of Turin: the history and legends of the world's most famous relic.* (R. A. Baylor University Press, 2019).

20. J. Beldon Scott, *Architecture for the Shroud: relic and ritual in Turin* (The University of Chicago Press).

21. A. Blanco-Míguez, *et al.*, Extending and improving metagenomic taxonomic profiling with uncharacterized species using MetaPhlAn 4. *Nat Biotechnol* **41**, 1633–1644 (2023).

22. X. J. Ching, *et al.*, Genome of a thermophilic bacterium Geobacillus sp. TFV3 from Deception Island, Antarctica.

23. A. L. Byrd, Y. Belkaid, J. A. Segre, The human skin microbiome. *Nat Rev Microbiol* **16**, 143–155 (2018).

24. N. S. Govind, A. T. Banaszak, Isolation and characterization of an autonomously replicating sequence (ARSD) from the marine yeast Debaryomyces hansenii. *Mol Mar Biol Biotechnol* **1**, 215–218 (1992).

25. P. Estrada-de Los Santos, P. Vinuesa, L. Martínez-Aguilar, A. M. Hirsch, J. Caballero-Mellado, Phylogenetic analysis of Burkholderia species by multilocus sequence analysis. *Curr Microbiol* **67**, 51–60 (2013).

26. P. Tahir, A. B. Ahmed, S. O. A. SaifulAzry, Z. Ahmed, Retting process of some bast plant fibres and its effect on fibre quality: a review. *Bioresources* **6**, 5260–5281 (2011).

27. A. Melelli, *et al.*, Lessons on textile history and fibre durability from a 4,000-year-old Egyptian flax yarn. *Nat. Plants* **7**, 1200–1206 (2021).

28. Z. Xu, *et al.*, Dandruff is associated with the conjoined interactions between host and microorganisms. *Sci Rep* **6**, 24877 (2016).

29. G. Sonnante, D. Pignone, K. Hammer, The Domestication of Artichoke and Cardoon: From Roman Times to the Genomic Age. *Annals of Botany* **100**, 1095–1100 (2007).

30. S. Mahr, Cardoon, Cynara cardunculus. *Wisconsin Horticulture - Division of Extensons - University of Wisconsin (Madison, USA)* (2025). Available at: https://hort.extension.wisc.edu/articles/cardoon-cynara-cardunculus/#:~:text=Cardoon%20is%20still%20cultivated%20for,was%20domesticated%20in%20ancient%20times [Accessed 15 April 2025].

1024 31. P. Tatke, R. Waghmare, “Antidiabetic plants with insulin mimetic activity” in
1025 *Antidiabetic Medicinal Plants*, (Elsevier, 2024), pp. 491–513.

1026 32. G. Grubben, O. Denton, *Plant resources of tropical Africa vegetables 2* (PROTA
1027 Foundation/Backhuys Publishers/CTA, 2004).

1028 33. M. Delplancke, *et al.*, Evolutionary history of almond tree domestication in the
1029 Mediterranean basin. *Molecular Ecology* **22**, 1092–1104 (2013).

1030 34. S. Kafkas, *et al.*, Pistachio genomes provide insights into nut tree domestication and
1031 ZW sex chromosome evolution. *Plant Communications* **4**, 100497 (2023).

1032 35. M. E. Kislev, A. Hartmann, O. Bar-Yosef, Early Domesticated Fig in the Jordan
1033 Valley. *Science* **312**, 1372–1374 (2006).

1034 36. J. Li, *et al.*, Maple phylogeny and biogeography inferred from phylogenomic data. *J*
1035 *of Sytematics Evolution* **57**, 594–606 (2019).

1036 37. D. Koeppel, *Banana: the fate of the fruit that changed the world* (Hudsen Street
1037 Press, 2008).

1038 38. M. Frei, “Il passato della Sindone alla luce della palinologia” in *La Sindone e La*
1039 *Scienza*, P. Coero-Borga, Ed. (Edizioni Paoline, 1979), pp. 191–200.

1040 39. M. Frei, “Identificazione e classificazione dei nuovi pollini della Sindone” in *La*
1041 *Sindone, Scienza e Fede*, (CLUEB, 1983), pp. 277–284.

1042 40. A. Danin, J. Baruch, “Floristic indicators for the origin of the Shroud of Turin” in *The*
1043 *Shroud of Turin/Unraveling the Mystery/Proceedings of the 1998 Dallas Symposium*,
1044 (Alexander Books, 2001), pp. 202–214.

1045 41. A. L. Price, *et al.*, Principal components analysis corrects for stratification in
1046 genome-wide association studies. *Nat Genet* **38**, 904–909 (2006).

1047 42. R. Cattaneo-Vietti, *et al.*, An overexploited Italian treasure: past and present
1048 distribution and exploitation of the precious red coral *Corallium rubrum* (L., 1758)
1049 (Cnidaria: Anthozoa). *Italian Journal of Zoology* **83**, 443–455 (2016).

1050 43. M. Iorizzo, *et al.*, Genetic structure and domestication of carrot (*Daucus carota*
1051 subsp. sativus) (Apiaceae). *American Journal of Botany* **100**, 930–938 (2013).

1052 44. O. Banga, Origin of the European cultivated carrot. *Euphytica* **6**, 54–63 (1957).

1053 45. O. Banga, Origin and distribution of the western cultivated carrot. *Genetica Agraria*
1054 357–370 (1963).

1055 46. K. Coe, *et al.*, Population genomics identifies genetic signatures of carrot
1056 domestication and improvement and uncovers the origin of high-carotenoid orange
1057 carrots. *Nat. Plants* **9**, 1643–1658 (2023).

1058 47. D. Langgut, The Citrus Route Revealed: From Southeast Asia into the
1059 Mediterranean. *HortScience* **52**, 814–822 (2017).

1060 48. Piero Coero-Borga, *La Sindone e la Scienza - Bilanci e Programmi - Atti del II*
1061 *Congresso Internazionale di Sindologia 1978* (Edizioni Paoline, 1978).

1062 49. M. R. Capodiferro, *et al.*, Archaeogenomic distinctiveness of the Isthmo-Colombian
1063 area. *Cell* **184**, 1706–1723 (2021).

1064 50. N. Rohland, E. Harney, S. Mallick, S. Nordenfelt, D. Reich, Partial uracil–DNA–
1065 glycosylase treatment for screening of ancient DNA. *Phil. Trans. R. Soc. B* **370**,
1066 20130624 (2015).

1067 51. Illumina, BLC Convert. (2023). Deposited 2023.

1068 52. M. Schubert, S. Lindgreen, L. Orlando, AdapterRemoval v2: rapid adapter trimming,
1069 identification, and read merging. *BMC Res Notes* **9**, 88 (2016).

1070 53. H. Li, R. Durbin, Fast and accurate short read alignment with Burrows–Wheeler
1071 transform. *Bioinformatics* **25**, 1754–1760 (2009).

1072 54. M. Schubert, *et al.*, Improving ancient DNA read mapping against modern reference
1073 genomes. *BMC Genomics* **13**, 178 (2012).

1074 55. H. Li, *et al.*, The sequence alignment/map format and SAMtools. *Bioinformatics* **25**,
1075 2078–2079 (2009).

1076 56. A. Peltzer, *et al.*, EAGER: efficient ancient genome reconstruction. *Genome Biol* **17**,
1077 60 (2016).

1078 57. G. Jun, M. K. Wing, G. R. Abecasis, H. M. Kang, An efficient and scalable analysis
1079 framework for variant extraction and refinement from population-scale DNA sequence
1080 data. *Genome Res.* **25**, 918–925 (2015).

1081 58. K. Okonechnikov, A. Conesa, F. García-Alcalde, Qualimap 2: advanced multi-
1082 sample quality control for high-throughput sequencing data. *Bioinformatics* **32**, 292–294
1083 (2016).

1084 59. H. Jónsson, A. Ginolhac, M. Schubert, P. L. F. Johnson, L. Orlando,
1085 mapDamage2.0: fast approximate Bayesian estimates of ancient DNA damage
1086 parameters. *Bioinformatics* **29**, 1682–1684 (2013).

1087 60. P. Skoglund, J. Storå, A. Götherström, M. Jakobsson, Accurate sex identification of
1088 ancient human remains using DNA shotgun sequencing. *Journal of Archaeological*
1089 *Science* **40**, 4477–4482 (2013).

1090 61. A. Mittnik, C.-C. Wang, J. Svoboda, J. Krause, A molecular approach to the sexing
1091 of the triple burial at the upper Paleolithic site of Dolní Věstonice. *PLoS ONE* **11**,
1092 e0163019 (2016).

1093 62. R. M. Andrews, *et al.*, Reanalysis and revision of the Cambridge reference
1094 sequence for human mitochondrial DNA. *Nat Genet* **23**, 147 (1999).

1095 63. A. Peltzer, Circular Mapper. (2020). Deposited 2020.

1096 64. H. Weissensteiner, *et al.*, Contamination detection in sequencing studies using the
1097 mitochondrial phylogeny. *Genome Res.* **31**, 309–316 (2021).

1098 65. T. S. Korneliussen, A. Albrechtsen, R. Nielsen, ANGSD: analysis of Next
1099 Generation Sequencing data. *BMC Bioinformatics* **15**, 356 (2014).

1100 66. S. Schönherr, H. Weissensteiner, F. Kronenberg, L. Forer, Haplogrep 3 - an
1101 interactive haplogroup classification and analysis platform. *Nucleic Acids Research* **51**,
1102 W263–W268 (2023).

1103 67. Q. Fu, *et al.*, A revised timescale for human evolution based on ancient
1104 mitochondrial genomes. *Current Biology* **23**, 553–559 (2013).

1105 68. Y. Huang, H. Ringbauer, hapCon: estimating contamination of ancient genomes by
1106 copying from reference haplotypes. *Bioinformatics* **38**, 3768–3777 (2022).

1107 69. S. Chen, Y. Zhou, Y. Chen, J. Gu, fastp: an ultra-fast all-in-one FASTQ
1108 preprocessor. *Bioinformatics* **34**, i884–i890 (2018).

1109 70. Md. Vasimuddin, S. Misra, H. Li, S. Aluru, Efficient architecture-aware acceleration
1110 of BWA-MEM for multicore systems in *2019 IEEE International Parallel and Distributed*
1111 *Processing Symposium (IPDPS)*, (IEEE, 2019), pp. 314–324.

1112 71. Broad Institute, Picard Toolkit. (2019). Deposited 2019.

1113 72. B. S. Pedersen, A. R. Quinlan, Mosdepth: quick coverage calculation for genomes
1114 and exomes. *Bioinformatics* **34**, 867–868 (2018).

1115 73. E. Alaçamlı, *et al.*, READv2: advanced and user-friendly detection of biological
1116 relatedness in archaeogenomics. *Genome Biol* **25**, 216 (2024).

1117 74. A. B. Rohrlach, J. Tuke, D. Popli, W. Haak, BREADR: an R package for the
1118 Bayesian estimation of genetic relatedness from low-coverage genotype data. [Preprint]
1119 (2023). Available at: http://biorxiv.org/lookup/doi/10.1101/2023.04.17.537144 [Accessed
1120 10 April 2025].

1121 75. D. Popli, S. Peyrégne, B. M. Peter, KIN: a method to infer relatedness from low-
1122 coverage ancient DNA. *Genome Biol* **24**, 10 (2023).

1123 76. S. Schiffels, SequenceTools. (2023). Deposited 2023.

1124 77. M. Martin, Cutadapt removes adapter sequences from high-throughput sequencing
1125 reads. *EMBnet.journal* **17**, 10–12 (2011).

1126 78. D. E. Wood, J. Lu, B. Langmead, Improved metagenomic analysis with Kraken 2.
1127 *Genome Biol* **20**, 257 (2019).

1128 79. J. Lu, *et al.*, Metagenome analysis using the Kraken software suite. *Nat Protoc* **17**,
1129 2815–2839 (2022).

1130 80. W. Shen, H. Ren, TaxonKit: A practical and efficient NCBI taxonomy toolkit. *Journal*
1131 *of Genetics and Genomics* **48**, 844–850 (2021).

1132 81. W. Shen, B. Sipos, L. Zhao, SeqKit2: A Swiss army knife for sequence and
1133 alignment processing. *iMeta* **3**, e191 (2024).

1134 82. D. Li, C.-M. Liu, R. Luo, K. Sadakane, T.-W. Lam, MEGAHIT: an ultra-fast single-
1135 node solution for large and complex metagenomics assembly via succinct de Bruijn
1136 graph. *Bioinformatics* **31**, 1674–1676 (2015).

1137 83. C. Camacho, *et al.*, BLAST+: architecture and applications. *BMC Bioinformatics* **10**,
1138 421 (2009).

1139 84. E. W. Sayers, *et al.*, Database resources of the national center for biotechnology
1140 information. *Nucleic Acids Research* **50**, D20–D26 (2022).

1141 85. D. J. Winter, rentrez: An R package for the NCBI eUtils API. *The R Journal* **9**, 520–
1142 526 (2017).

1143 86. R. Kolde, pheatmap: Pretty Heatmaps. (2018). Deposited 2018.

1144 87. A. McKenna, *et al.*, The Genome Analysis Toolkit: A MapReduce framework for
1145 analyzing next-generation DNA sequencing data. *Genome Res.* **20**, 1297–1303 (2010).

1146 88. R Core Team, R: A language and environment for statistical computing. (2021).
1147 Deposited 2021.

1148 89. Wickham H (2016). ggplot2: Elegant Graphics for Data Analysis. Springer-Verlag New
1149 York. ISBN 978-3-319-24277-4, https://ggplot2.tidyverse.org

Figures and Tables

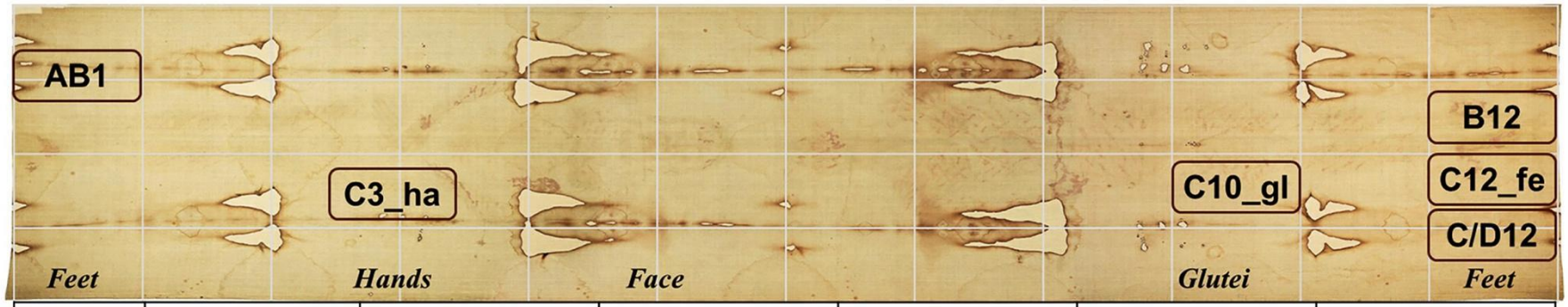

Sample ID	Specimen	Human Content (%)	Human nDNA Average Depth (X)	Human mtDNA Average Depth (X)	Human mtDNA haplogroup(s)	N. Human mtDNA heteropl.s (>0.01)
AB1	*Linen fragment*	*47.18*	*1.38*	*147.13*	*K1a1b1a; H2a2*	*97*
B12	*Microscope slide*	*39.60*	*1.14*	*90.01*	*K1a1b1a; H33*	*58*
C3_ha	*Vacuum dust*	*1.93*	*0.05*	*4.49*	*U5a1 @16192*	*1*
C10_gl	*Vacuum dust*	*18.68*	*0.54*	*52.96*	*K1a1b1a; H1b*	*21*
C12_fe	*Vacuum dust*	*0.05*	*0.00*	*0.35*	*H2a2a1*	*2*
C/D12	*Linen fragment*	*5.64*	*0.10*	*13.23*	*K1a1*	*0*
R58	*Linen fragments from Reliquary*	*0.57*	*0.02*	*4.04*	*K1a1b1a*	*0*

Figure 1. Summary of the human genomic data obtained from the TS samples. See Table S1, Figure S1, and Dataset S1 for further details.

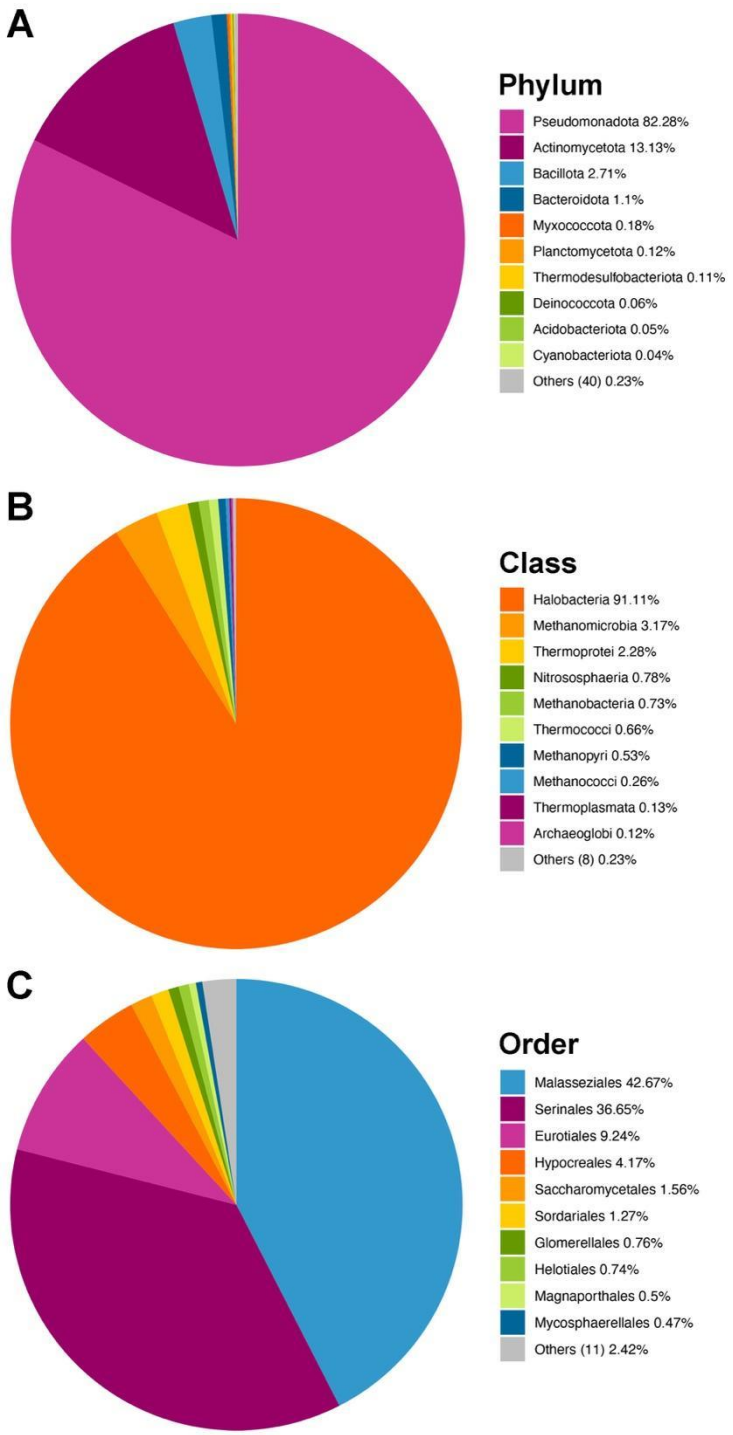

Figure 2. Cumulative taxonomic assignment of the TS reads. The results show the relative abundance of the bacterial phyla (A), archaeal classes (B), and fungal orders (C).

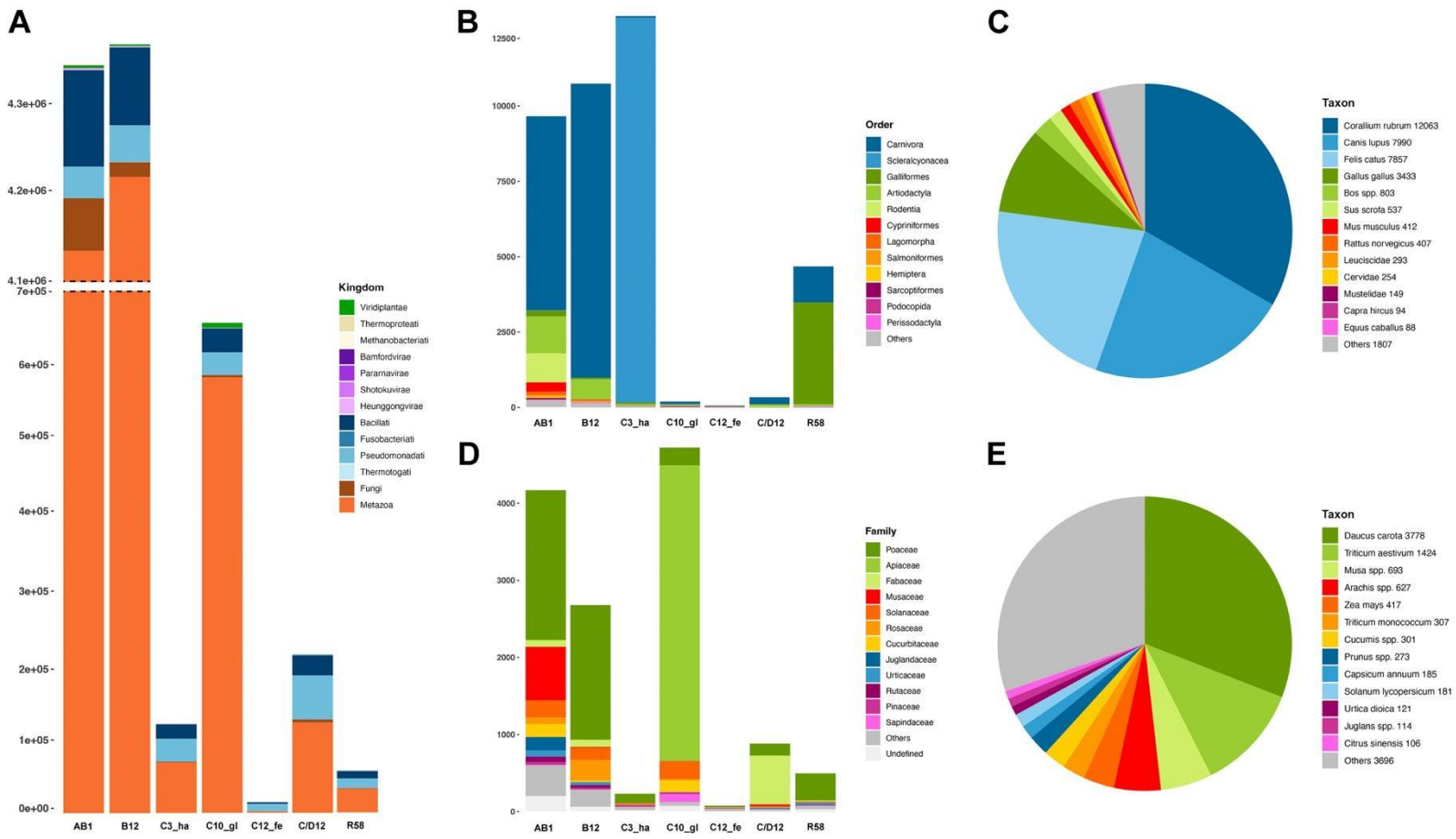

Figure 3. Graphical summary of the results of the taxonomic assignment of contigs. Number of contigs for each TS sample and their distribution among kingdoms (A), orders of Metazoa (B), assigned taxa of Metazoa (C), families of Viridiplantae (D), assigned taxa of Viridiplantae (E).

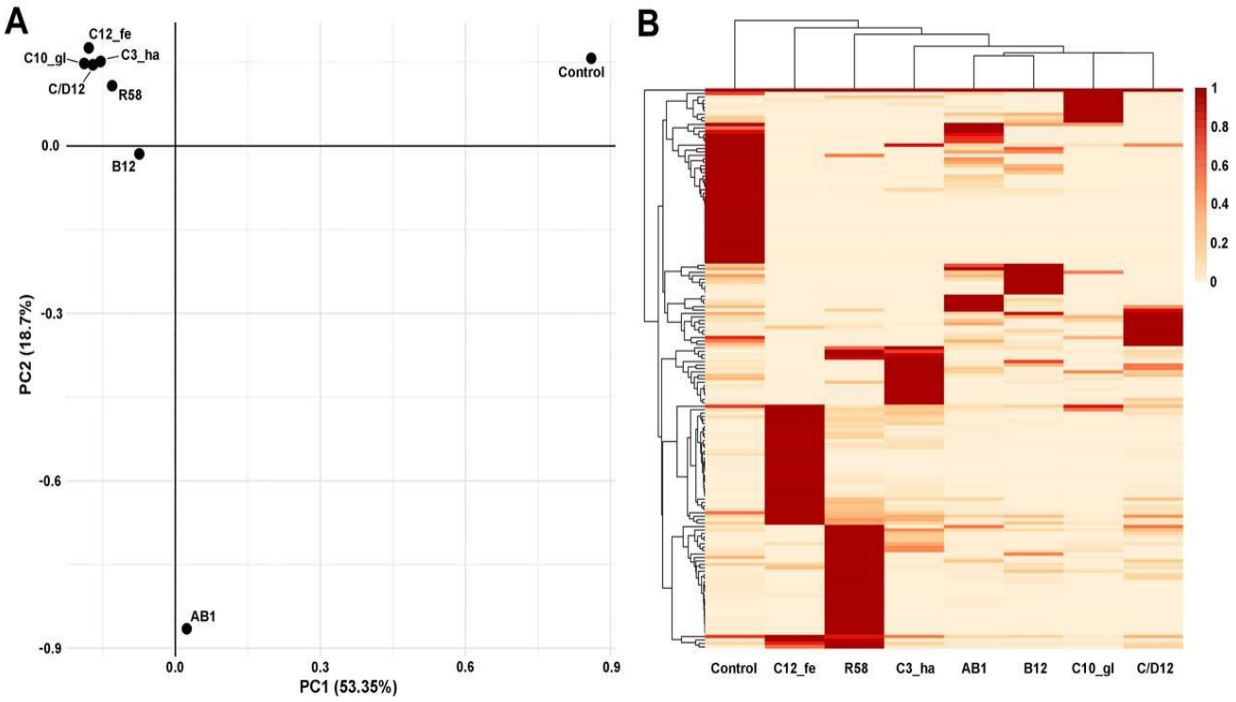

Figure 4. Clustering analyses. (A) Principal Component Analysis and (B) Hierarchical Clustering based on BLASTn metagenomic data of the seven TS samples and an artificially contaminated linen fragment (control).

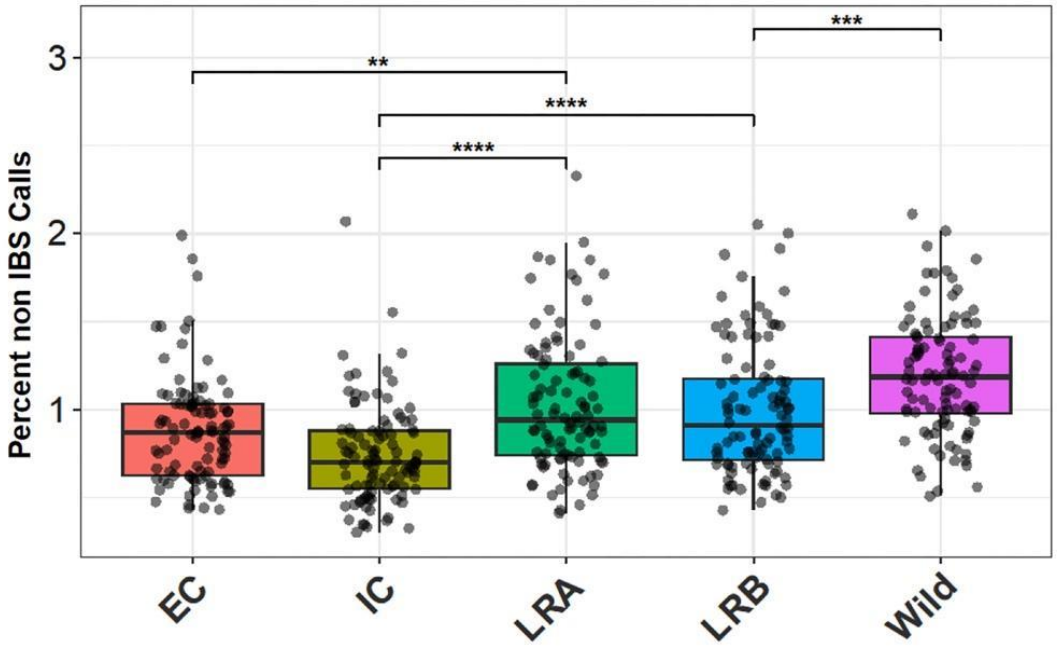

Figure 5. Percent of non-Identical By State (IBS) calls between contigs assembled from C10_gl sample and carrot population groups. Carrot samples represent the following populations as determined by Coe et al. (46): Early cultivars (EC), Improve cultivars (IC), Landrace A, Landrace B and Wild. Each data point represents a random subset of 20 contigs sampled from 1,787 contigs. Significant differences were tested using T-Test. Asterisks represent the following significant levels: *=0.05, **=0.01, ***=0.001, ****=0.0001.